POLITECNICO MILANO 1863

DIPARTIMENTO DI MECCANICA

Impact tests of wheels of road vehicles: a comprehensive method for numerical simulation

F. Ballo, G. Previati, G. Mastinu, F. Comolli

This is a post-peer-review, pre-copyedit version of an article published in journal title. The final authenticated version is available online at: http://dx.doi.org/10.1016/j.ijimpeng.2020.103719

DIPARTIMENTO DI MECCANICA ■ POLITECNICO DI MILANO
via G. La Masa, 1 ■ 20156 Milano ■ EMAIL (PEC): pecmecc@cert.polimi.it
http://www.mecc.polimi.it
Rev. 0

Impact tests of wheels of road vehicles: a comprehensive method for numerical simulation

F. Ballo, G. Previati, G. Mastinu, F. Comolli

Politecnico di Milano, Department of Mechanical Engineering,Via La Masa 1, Milan

---

Abstract

In the design of automotive wheels, safety is a crucial factor. Homologations, legislation and standards require severe impact tests before a new wheel can be released on the market. Impact tests are usually performed after the wheel has been already designed and the first prototypes have been produced. In case of test failure, significant delays and costs have to be sustained before the wheel can be actually produced. Numerical simulation of wheel impact tests can reduce the risk of test failure and be a valuable tool for the designer to obtain more efficient and light wheels. The paper deals with the full digitalization of the design process of road vehicle wheels. The aim is to reduce as much as possible indoor impact tests to assess wheel rim structural safety. The numerical simulation of impact tests is accomplished by complex finite element models comprising wheel, tyre and test rig structure. Several data can be required for the modelling of the tyre, which are not usually known to the wheel designer. In this paper, a method for the realization of finite element models of different impact tests is presented. By the proposed method, finite element models with a sufficient level of accuracy for the design of the wheel, at a relatively low computational cost, can be obtained by means of a well defined procedure. For tyre characterisation, only simple measurements related to geometrical features, stiffness and frequency response are required.

The method is successfully applied to different impact tests such as radial impact tests with flat or V-shaped striker and 13° side impact test. For all the considered tests, experimental validations are performed on different wheels, instrumented with strain gauges located at the most stressed areas. The striker accelerations are also reproduced accurately.

The method for the numerical simulation of indoor impact tests of road vehicle wheels enables the full digitalisation of design process, with relevant results in terms of ”time to market” reduction and structural safety assessment. The proposed method is useful not only to design wheel rims, but also to design pneumatic tyres.

Keywords: Radial impact, Lateral impact, Aluminium wheel, Numerical simulation

1. Introduction

One billion road vehicles are running on the globe. The yearly turnover of transport in the world is 7000 billion dollars. One million deaths are due to road accidents. The research presented in this paper has an impact on the mentioned figures [1]. Actually, the design of wheel rims deserves special attentions due to high production volumes. The lighweight design has an impact on transport budget, which is extremely high. Safety of transport is a basic issue which implies structural design of wheel rims.

In the design of automotive wheels, safety is a crucial factor. Homologations, legislation and standards require severe impact tests before a new wheel can be released on the market. Impact tests are usually performed after the wheel has been already designed and the first prototypes have been produced. In case of test failure, significant delays and costs have to be sustained before the wheel can be actually produced. Numerical simulation of wheel impact tests can reduce the risk of test failure and be a valuable tool for the designer to obtain more efficient and light wheels.

Numerical simulation of impact test refers to creating ”digital twins” of test rigs. Such a digitalisation is one of the paradigms of *Industry 4.0*. The digitalisation of the design process allows quicker and cheaper and safer activities focused on ”time to market” reduction, a fundamental goal of automotive industry.

Europe is the leading country in the world for investments in automotive R&D. Nearly 50 billion Euro/year are invested. Much of such amount of money is devoted to make the development of products and related production processes more efficient. The paper aims to give a contribution in this area.

Wheels are crucial components for vehicle safety and performance. Referring to safety, wheels, by bearing the loads coming from road surface, clearly have a primary role and a failure of the wheel could result in a sudden loss of control of the vehicle.

Concerning performance, wheels have effects on handling and on fuel consumption. In fact, since the wheel constitutes a relevant portion of the unsprung mass, a lightweight design of the wheel results in better road holding performances of the car [2].

Lightweight design of wheels is also fundamental for mass reduction, which plays a fundamental role in the framework of fuel consumption and GHG (Greenhouse Gas) emission minimisation. Important studies have claimed that a 10% reduction in the vehicle mass results in a reduction of the fuel consumption that ranges from 8% to 9% depending on the type of vehicle [3, 4].

For the durability assessment of wheels, different types of fatigue tests are prescribed. In the rotary bending fatigue test [5, 6], the wheel is subject to a rotating bending moment. The wheel is tested without the tyre and is clamped at the inner rim flange. The bending moment is applied through a rotating mass acting on a central shaft fastened at the wheel hub. In the biaxial fatigue test [7, 8, 9], the wheel and tyre assembly is left to rotate on a rolling drum; different combinations of vertical and lateral forces are applied according to well defined load sequences [10].

Beside fatigue tests, impact tests are also prescribed to replicate the most severe forces acting on the wheels. These tests are meant to simulate critical loading conditions such as impact with road pot-holes, kerbs or other concentrated obstacles. Different types of impact tests are used, either prescribed by standards [11, 12], or defined by vehicle manufacturers [13].

Among the available impact tests, the most common ones are the radial impact test, with flat or V-shaped strikers [13], and side impact tests typically with a 13° impact angle [11, 12]. In the literature, a certain number of papers dealing with the numerical simulation of such tests can be found.

A large variety of numerical models of the 13° side impact test have been proposed in the literature [14, 15, 16, 17, 18, 19]. In all those references, finite-element based models have been employed for the numerical simulations. In the models, the tyre, rim, striker and supporting structure are generally included and the numerical simulation is carried out by means of an explicit solver. It is acknowledged [14] that tyre modelling constitutes the most relevant and complex part of the process. An accurate modelling of the tyre requires a deep knowledge of the actual structure and of the rubber materials that compose the tyre carcass [14]. To overcome this difficulty, some attempts have been made to develop a simplified approach for the numerical modelling of the 13° side impact test [17, 20]. In [17], the simplification consists in removing the tyre from the model and in reducing the kinetic energy of the striker by 20% to compensate the tyre absence. In [20], the authors propose a simplified model based on a static simulation with an equivalent load equal to 10 times the weight of the striker.

Regarding the study of the radial impact test, few references can be found in the literature. In this kind of test, different supporting structures, striker shapes and striker positioning with respect to the tyre can be found. In [21], the 90° (radial) impact test of a steel wheel is simulated through a finite-element model. In this test, a 90° V-shaped striker hitting half of the tyre width is considered. The numerical model comprises all the main components, i.e. the tyre, wheel, striker and support structure. The actual structure of the tyre is modelled, made up by five different rubber materials and three different layers of reinforcements embedded in the rubber carcass. Experimental results presented in the paper, confirm that the size and structure of the tyre have a strong influence on the response to the impact test. In [22] the authors study the 90° radial impact test of a cast aluminium alloy wheel. In this case, the striker has a flat shape - a simplified finite element model made up by the wheel (without tyre) and the striker is developed. The dynamic impact response of the wheel is simulated by means of explicit finite element analyses and a comparative numerical study on wheels with different number of spokes was carried out in the paper. In [23], both the 90° radial impact with flat striker and the 13° side impact test are simulated by means of Abaqus ® Explicit. In the numerical models, the wheel, tyre, striker and supporting structures are included.

In [24], the authors investigate the response of a steel wheel to a mixed radial/lateral impact test (35° impact test). In this case a simplified model of the tyre structure is employed. The model consists of a rubber carcass described by a single hyperelastic Mooney-Rivlin material, the bead core is modelled with a solid isotropic material and rebar layers are used to model the carcass ply and the steel plies. An explicit solver is used to simulate the impact test.

In the present paper, a method for the construction of finite element models suitable for the simulation of different impact tests on aluminum wheels is presented. The resulting models have a sufficient level of detail for the design of the wheel while keeping at a minimum the simulation time and the data required for the characterization of the tyre. The method is derived by extending the approach proposed by some of the authors in [25, 26] referring to the simulation of a radial impact test with a V-shaped striker [13]. The finite element model presented in the paper comprises tyre, aluminium wheel, striker and support structure. The tyre has been modelled by a simplified model considering different rubber materials for sidewall, undertread and tread. Belt and carcass plies are also considered. The geometry of the tyre is measured by a 3D measuring arm, while the material and reinforcement properties are taken from the literature and tuned by means of deflection and frequency response tests. In the present paper, this model is extended to consider different impact tests. Also, contrary to usual solution approaches in the literature, for some impact configurations, the possibility to use an implicit solver to increase the stress accuracy is explored.

The method proposed in this paper is not only relevant for industry focused on wheel manufacturing, but also for tyre manufacturers [27, 28, 29]. Actually, studying the structural safety of tyres is strictly related to the safety of wheel rims.

The paper is structured as follows. In the next section the impact tests considered in the paper are described. Then, in Sect. 3 the structure of the proposed model is described, along with the modelling approaches for the considered components (tyre, wheel, support structure and striker). In this section, also some consideration about the use of implicit or explicit solvers are reported. Finally, section 4 presents the experimental tests performed on real impact test benches and the validation of the numerical models for the considered impacts.

2. Impact test descriptions

In this section, the three impact tests considered in this paper are described. The proposed method has been tested with reference to these tests, but it can be easily applied also to different impact conditions.

2.1. Radial impact test, V-shaped striker

In the radial impact test with V-shaped striker [13], the wheel is fixed to a supporting structure as shown in Figure 1. The supporting structure realizes a compliant mechanism composed by a hinge constraint and a calibrated spring. During the test, a falling mass radially hits the tyre tread; the striker, i.e. the portion of the falling mass directly in contact with the tyre, has the V-shaped profile shown in Figure 2. Additionally, in the test, the position of the supporting structure is adjusted so as to have an angle of 1° between the edge of the striker and the tyre tread. The energy level depends on the size of the wheel to be tested and is adjusted by modification of the striker mass and its falling height.

2.2. Radial impact test, flat striker

In the radial impact test with flat striker, the wheel is fixed to a rigid supporting structure and a falling mass hits the tyre tread along the radial direction. The striker's shape is flat in this case and is parallel to the tread surface. The

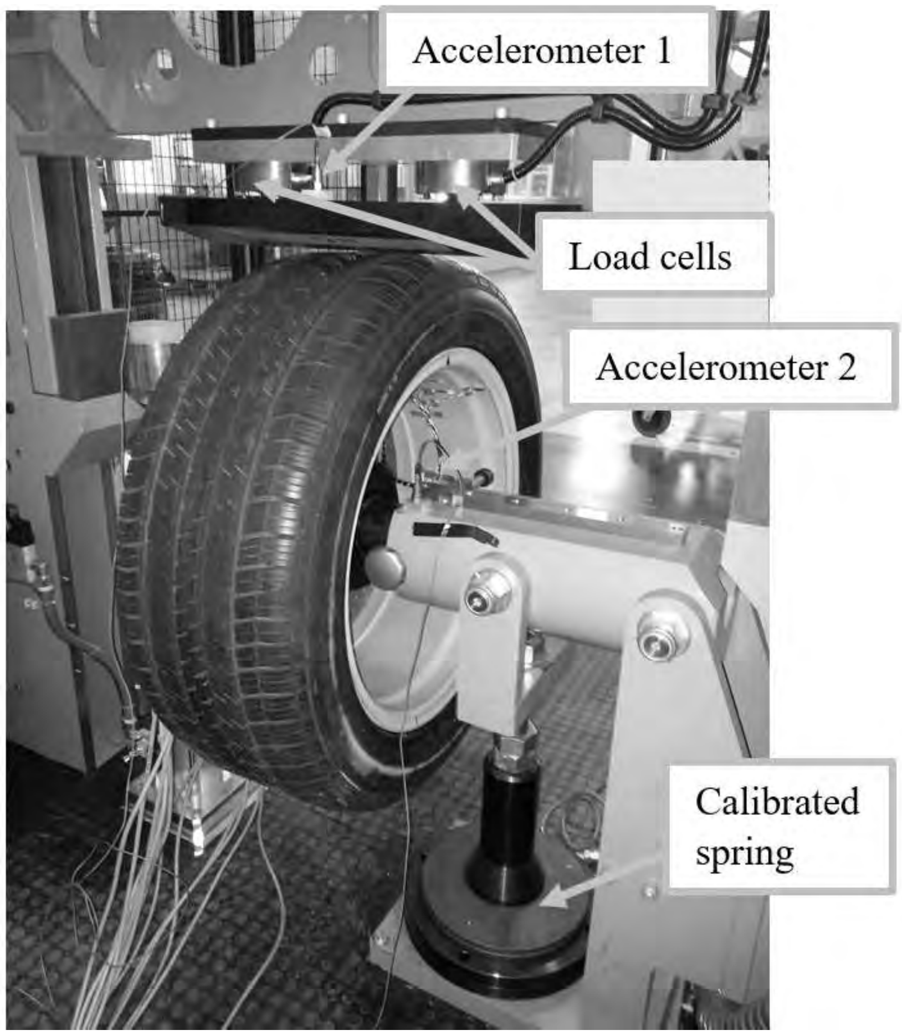

Figure 1: Typical setup of the radial impact test with V-shaped striker, in the figure also piezoelectric accelerometers used for experimental validation are highlighted. Courtesy of "Cromodora Wheels".

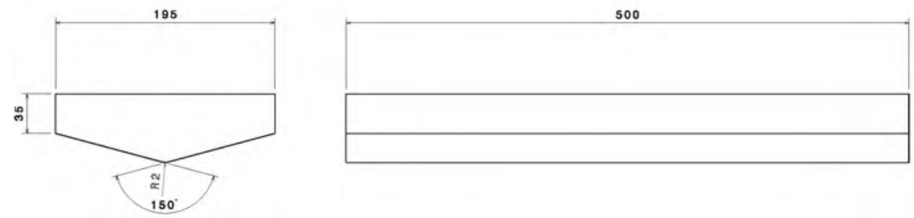

Figure 2: Geometry of the V-shaped striker of the radial impact test, dimensions are in mm.

energy level depends on the size of the wheel to be tested and is adjusted by modification of the striker mass and its falling height. Figure 3 depicts the typical test layout of the radial impact test with flat striker.

2.3. 13° *side impact test*

In the 13° side impact test, described by SAE J175 and ISO 7141 standards [11, 12], the wheel and tyre assembly are oriented of an angle equal to 13° w.r.t. the plane of the striker as shown in Figure 4. The striker impacts the tyre sidewall and the outer rim flange. The wheel is fixed to a compliant structure supported by four calibrated rubber bumpers. The energy level depends on the size of the wheel to be tested and is adjusted by modification of the striker mass and its falling height.

3. Finite element model of impact tests

The finite element models used to simulate the different impact tests share the same structure and modelling approach. The models comprise tyre, wheel, striker and support structure. Of these elements, wheel and tyre are common to all models and will be described in Sect. 3.1 and Sect. 3.2. The strikers present different shapes depending on the test type but are all modelled as rigid surfaces. The strikers are positioned close to the tyre and an initial velocity, corresponding to the pertinent falling height, is assigned at the beginning of the simulation. To the strikers, a concentrated mass of the correct value is attached to obtain the desired impact energy. Finally, the supporting structure

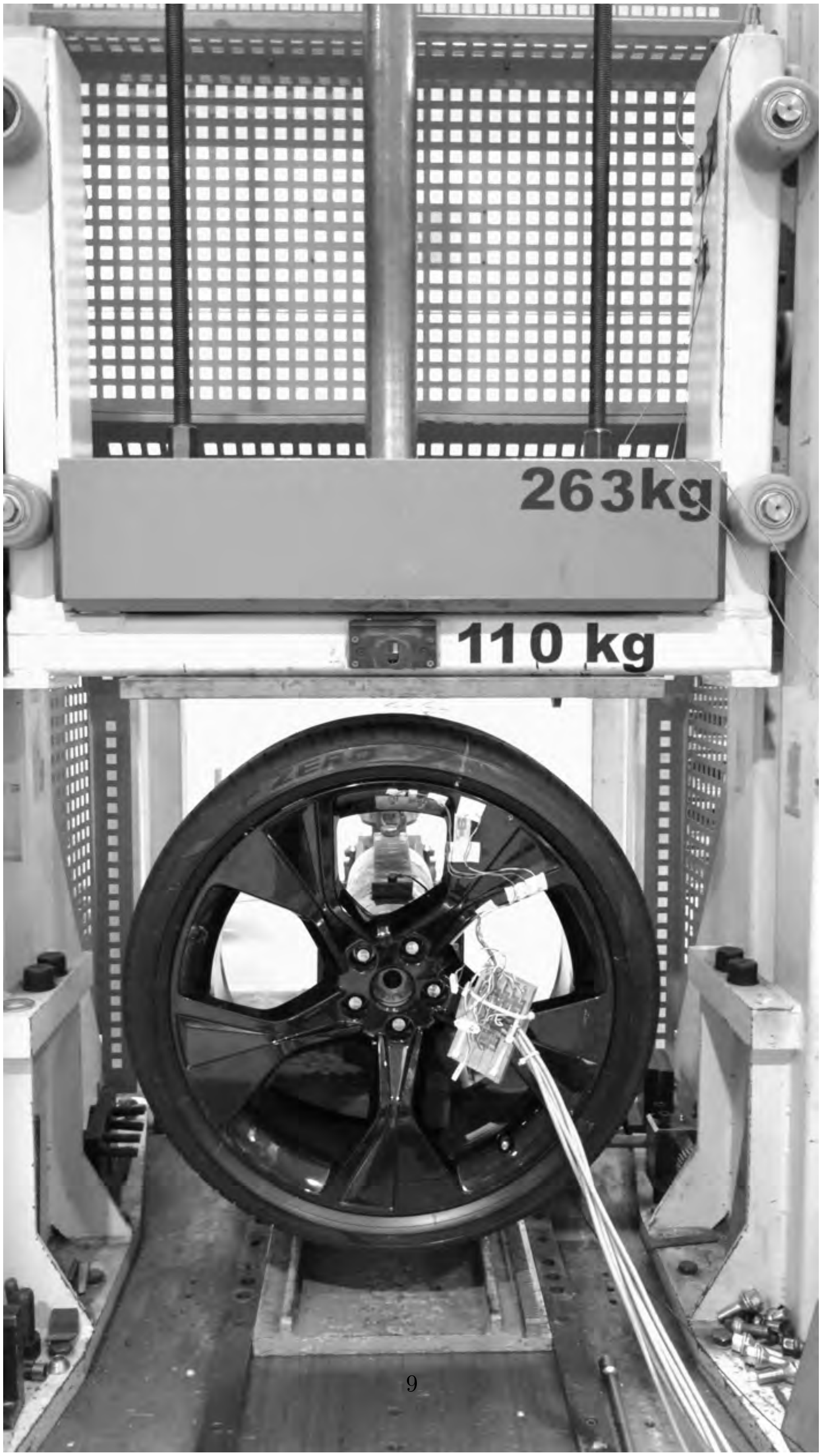

Figure 3: Typical setup of the radial impact test with flat striker, in the figure an instrumented wheel used for the experimental validation is shown. Courtesy of "Cromodora Wheels".

Figure 4: Typical setup of the 13° side impact test, in the figure an instrumented wheel used for experimental validation is shown. Courtesy of "Cromodora Wheels".

is different for each impact test and is modelled accordingly as shown in Sect. 3.3.

The solution strategy is the same for all models. The analysis is divided in two steps. A first step, in which the tyre is inflated up to the desired pressure depending on the impact specification, followed by a second step where the actual impact is simulated. For the solution of the two steps, different solvers are employed. The first step is always solved by an implicit non linear solver. For the second step, either an implicit or explicit solver is used, depending on the impact type. The choice between these two kinds of solver depends on the amount of deformation of the tyre. In particular, if the tyre undergoes a large deformation and the convergence of an implicit solver is unlikely, an explicit solver is employed. In fact, explicit solvers can handle very large deformations and very complex contact conditions, impossible to solve by implicit ones. This situation is typical of radial-type impacts, where the tyre completely folds and complex contact conditions as well as severe deformations are present.

The drawbacks of the use of an explicit solver are mainly related to the required computational time and to the binding requirements on the mesh definition. Even if explicit solvers are the usual choice for impact simulations, in this particular case they may not be the best choice. In fact, due to the tyre and supporting structure compliance and the relatively low velocity of the striker, the impact has a relatively long duration, of the order of 0.1-0.2 s. The material of the wheel has high elastic modulus and, due to the complex wheel shape, small elements have to be used. The combination of high elastic modulus and small elements leads to a very small stable increment time [30]. This situation is also worsened by the geometry of the wheel that often does not allow for the realization of regular meshes, thus further reducing the stable integration step. As a result, integration steps as small as of the order of 10^{-8} s have to be used. Such small integration steps lead to relatively long computational times. Since the minimum stable integration step cannot be reduced to avoid excessive computational times, this limits the possibility to have small elements in sharp regions of the wheel and also limits the possibility to use quadratic elements.

This in turn results in limitations in the stress accuracy in some parts of the wheel. Finally, to avoid distorted elements, a quite long time is required for mesh preparation and usually selective mass scaling has to be employed.

A possible way to avoid such limitations is the use of an implicit solver. Implicit solvers are not usually employed for impacts due to convergence problems and to the difficulties in having a high frequency sampling of the solutions [30, 31]. In fact, in the literature no paper using an implicit solver for wheel impacts can be found. If the lateral impact is considered, however, the deformations of the tyre and of the wheel are not very large. Also contacts are relatively simple. In this situation, it is possible to use an implicit solver so as to have, locally, a finer mesh and improve the accuracy of the computed stress field. This kind of solver allows for a substantial reduction of the computational time because, even if each time increment is much more costly than that of an explicit solver, relatively few increments can be used. Time sampling is not a particular issue, as the system dynamics is quite slow. For such impact, it can be convenient to switch to an implicit solver both for reducing the computational time and to have a more refined mesh.

The test configurations of all of the considered impacts show a symmetry with respect to the midplane of the tyre. Such symmetry is exploited to reduce the dimension of the numerical model by modelling only half of the system. However, in some cases, the wheel is not symmetric. In this cases, the system is no longer symmetric and the model cannot be reduced.

3.1. Tyre model

In this section, the numerical modelling of the tyre is dealt with. The focus of the tyre model is not the study of the behaviour of the tyre itself during the impact, but the estimation of the effect of the tyre on the wheel. For this reason, a relatively simplified model is adopted for the tyre. Tyre data are not often available. To overcome this problem, the required data are obtained from direct measurements of the geometry of the tyre, from the literature and from simple deflection and frequency response tests.

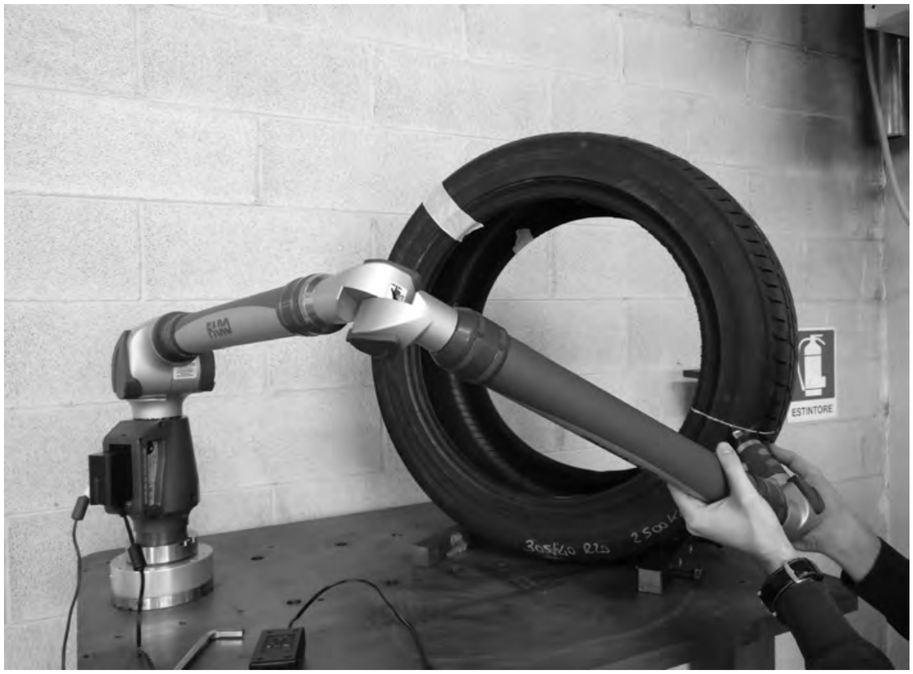

Figure 5: Measurement of tyre cross section through a "FARO" 3D measuring arm.

The geometrical features of the analysed tyres were reproduced starting from experimental measurements. The tyre cross section was measured by means of a "Faro" 3D measuring arm as shown in Figure 5; several points located on the outward and inward side of the tyre carcass were picked and used to reconstruct the geometry of the tyre for Finite Element modelling.

The tyre structure is modelled as depicted in Figure 6; the model consists of several main features, namely tread, undertread, sidewall, bead core, belt plies and body ply. The tread, undertread and sidewall are made of rubber material, described by a Mooney-Rivlin constitutive law. Different coefficients were adopted for each of these parts of the tyre structure to account for the different compounds they are realised with.

The Mooney-Rivlin coefficients of the rubber materials are derived starting from reference values taken from the literature [32], which are then adapted

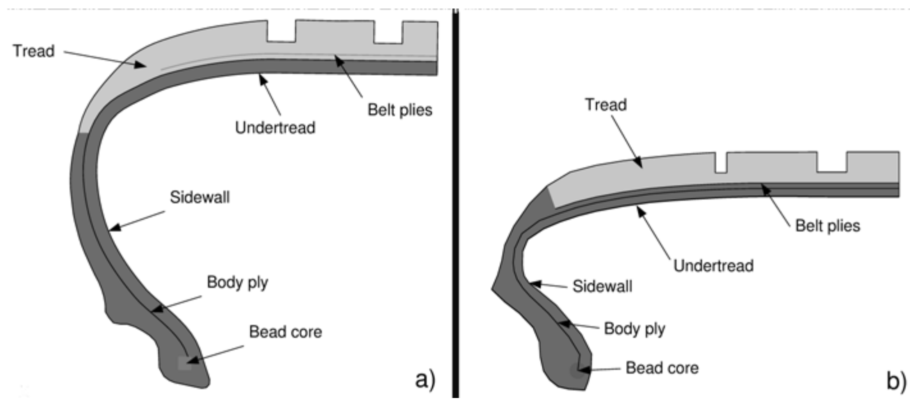

Figure 6: Numerical model of the tyre structure for the two different tyres considered in this paper a) 265/50 R19 b) 295/30 R20.

to the actual tyre under consideration by means of vertical and lateral static stiffness tests as described in [25, 33, 34]. Figure 7 depicts the comparison among simulated and experimental vertical stiffness tests for the two tyres considered in this paper (265/50 R19 and 295/30 R20 radial tyres), while in Figure 8 the comparison related to the lateral stiffness is shown.

The bead core can be described either by a 3D isotropic structure or by a 1D beam element with an equivalent circular cross section.

Reinforcement plies are embedded in the tyre carcass as shown in Figure 6, and are modelled by a series of equally spaced rebar elements. To completely define the properties of the ply, the cross sectional area and the spacing between the rebar elements need to be specified. The body ply is made from Nylon and has a 90 degrees (radial) orientation, while the belt plies are made from a symmetric steel ply stack oriented $\pm 20°$ with respect to the hoop direction.

All material and structural properties of the two considered tyres are summarised in Table 1 and Table 2.

Tyre damping is modelled through a Rayleigh model [35, 25], the model coefficients are identified through experimental modal tests on tyre tread and sidewall. In the tests, described in detail in [25, 26], the frequency response

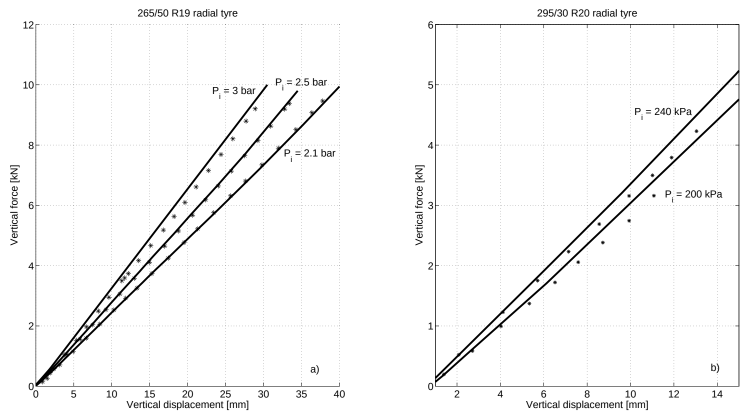

Figure 7: Comparison of vertical force/displacement graphs at different inflation pressures for a 265/50 R19 radial tyre (a) and a 295/30 R20 radial tyre (b). Solid lines are numerical simulations, asterisks are experiments.

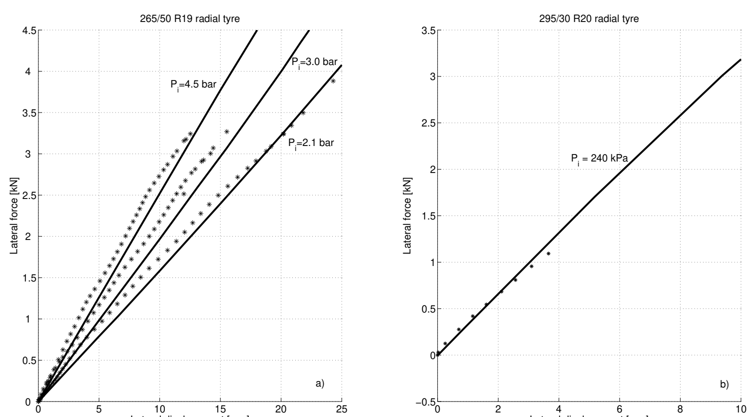

Figure 8: Comparison of lateral force/displacement graphs at different inflation pressures for a 265/50 R19 radial tyre (a) and a 295/30 R20 radial tyre (b). Solid lines are numerical simulations, asterisks are experiments.

Table 1: Material properties of the two considered tyres.

	Material type	Parameters
265/50 R19 radial tyre		
	Material type	Parameters
Steel	Linear elastic	$E = 210GPa, \nu = 0.3, \rho = 7800\frac{kg}{m^3}$
Nylon	Linear elastic	$E = 3.4GPa, \nu = 0.3, \rho = 1140\frac{kg}{m^3}$
Sidewall/undertread	Mooney-Rivlin	$C_{10} = 0.1MPa, C_{01} = 0.4MPa, \rho = 1100\frac{kg}{m^3}$
Tread	Mooney-Rivlin	$C_{10} = 0.14MPa, C_{01} = 1.8MPa, \rho = 1100\frac{kg}{m^3}$
295/30 R20 radial tyre		
	Material type	Parameters
Steel	Linear elastic	$E = 210GPa, \nu = 0.3, \rho = 7800\frac{kg}{m^3}$
Nylon	Linear elastic	$E = 3.4GPa, \nu = 0.3, \rho = 1140\frac{kg}{m^3}$
Sidewall/undertread	Mooney-Rivlin	$C_{10} = 0.7MPa, C_{01} = 1.4MPa, \rho = 1100\frac{kg}{m^3}$
Tread	Mooney-Rivlin	$C_{10} = 0.8MPa, C_{01} = 1.5MPa, \rho = 1100\frac{kg}{m^3}$

Table 2: Geometric properties of the plies of the two considered tyres.

265/50 R19 radial tyre		
	Wire spacing $[mm]$	Wire cross section $[mm^2]$
90 degree ply	1	0.4
±20 degree belts	1	0.2
295/30 R20 radial tyre		
	Wire spacing $[mm]$	Wire cross section $[mm^2]$
90 degree ply	1	0.4
±20 degree belts	1	0.2

Table 3: Identified Rayleigh's coefficients for the tread and the sidewall - 265/50 R19 radial tyre.

	α	β
Tread	43.9	$1.5e-6$
Sidewall	3.5	$1.2e-4$

functions of the tyre tread and sidewall are measured and damping of each eigenmode is estimated by means of the half-power bandwidth method. Rayleigh coefficients α and β are then identified through a least-square fitting on the measured data [25, 26], identified values are reported in Table 3.

3.2. Wheel model

The A356 T6 aluminium alloy wheel is modelled with an isotropic material; since during the test significantly large deformations occur on the wheel rim and spokes, the nonlinear elasto-plastic laws of Figure 9 are considered for the material response. Wheel material inhomogeneities, mainly due to different cooling rates in the different zones of the wheel, are considered in the numerical

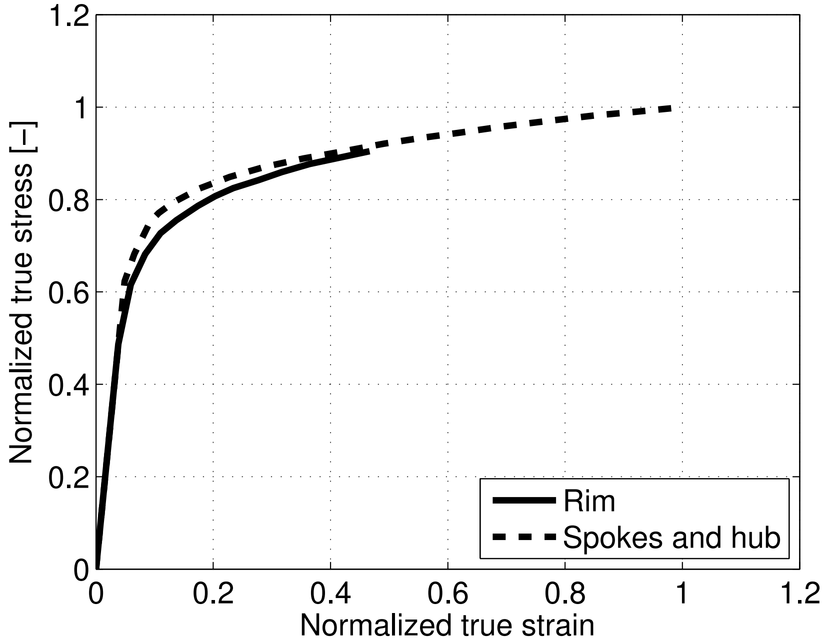

Figure 9: Material constitutive laws employed for the rim region (solid line) and for the spokes/hub region (dashed line). The two curves are normalized over the same values.

model [36]. Two distinct material constitutive curves are considered for the wheel rim and the wheel spokes (and central hub). The two material constitutive laws are highlighted in Figure 9 and have been obtained from tensile tests on specimens extracted from different areas of the spokes and the wheel rim.

The interaction between wheel and tyre is modelled by a frictional contact constraint with friction coefficient equal to 0.5 as suggested by [37].

3.3. Support structure models

The support structure varies for the different considered impact tests. In modelling the different structures, the same approach can be used. In most cases, the compliance of the support structure has a relevant influence on the impact test. For this reason, the support structure is usually modelled as a deformable body. However, the stress in the support structure is not of concern in the test. For this reason, a very coarse mesh can be used for the structure. In some cases, elastic elements are attached to the support structure to obtain a prescribed compliance. In these cases, particular care has to be given to the correct modelling of such elements and to the kinematic of the support structure. If the stiffness of the structure is much higher than the stiffness of the elastic elements, the structure can be modelled as a rigid body.

The interface between the wheel and the support structure is modeled as a rigid connection.

In the following subsections, the different support structures are described.

3.3.1. Radial impact test with V-shaped striker

In this impact test, as shown in Figure 1, the support structure realizes a kinematic mechanism and a calibrated spring is employed to have a prescribed vertical compliance. In this case, being the structural stiffness of the supporting structure significantly higher than the calibrated spring, the supporting structure has been modelled as a rigid body. By this constraint, the computational time is greatly reduced while the inertial effects of the structure are considered.

The resulting numerical model of the radial impact test with V-shaped striker is depicted in Figure 10, in which the geometry of the considered wheel has allowed the exploitation of the symmetry. The striker was modelled as a rigid surface with a concentrated mass and the geometry defined in Figure 2.

To complete the model, the following interactions and boundary conditions have been defined.

- Symmetry constraint at the meridian plane.
- The extreme of the supporting structure is fixed to the ground with a hinge constraint.
- The central part of the supporting structure is sustained by an axial spring with constant stiffness equal to 85 kN/mm (42.5 kN/mm in the half model).

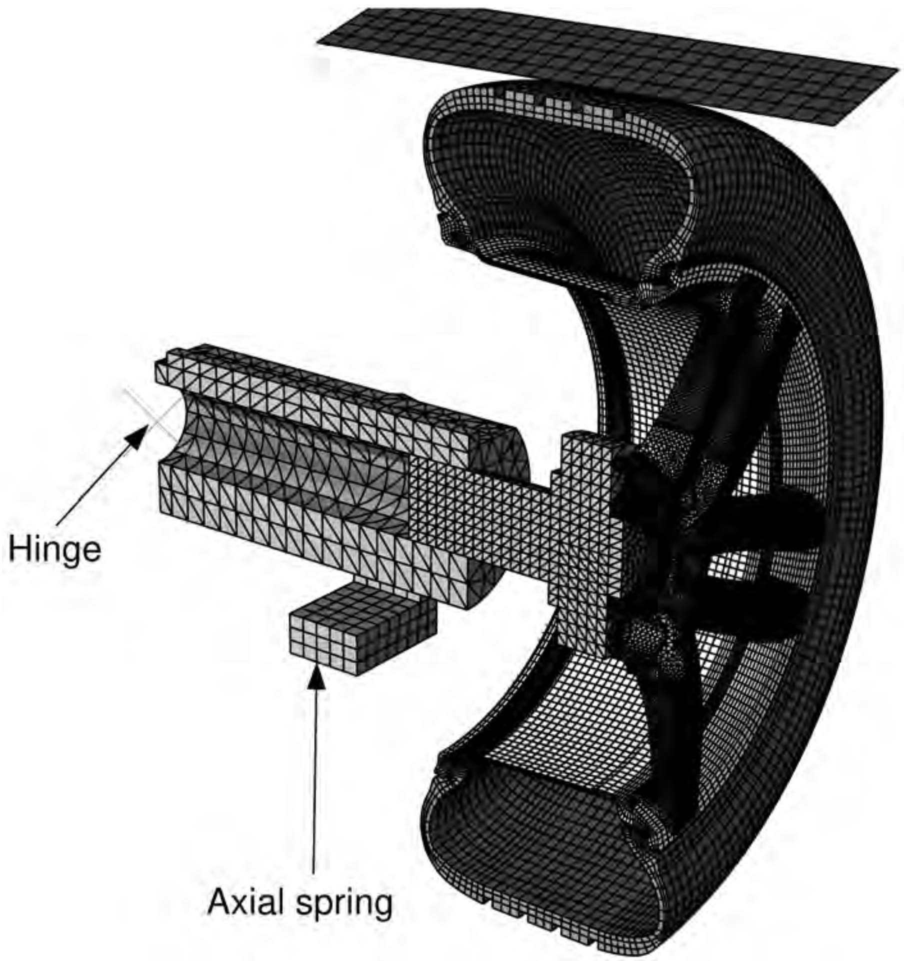

Figure 10: Numerical model of the radial impact test with V-shaped striker.

In the model shown in Figure 10, the tyre structure is discretised with 8-nodes brick elements with typical dimension of about 8mm, while the wheel rim and spokes are discretised with 4-nodes tetrahedrons with typical dimension of about 7mm. Great care was devoted to the definition of the finite element mesh in order to maximise the stable time increment in the explicit simulation. The smallest stable time increment obtained is of $1.65 \cdot 10^{-8}$ s, the total duration of the simulation step is set long enough to model the total compression and spring-back phase.

3.3.2. Radial impact test with flat striker

For this impact test, the support structure is rigidly connected to the ground (Figure 3). In order to account for the (small) compliance of the structure during the test, the supporting structure is modelled as a deformable body.

The resulting model is shown in Figure 11. The mesh of the supporting strucure is very coarse. The tyre structure is discretised with 8-nodes brick elements with typical dimension of about 8mm, while the wheel rim and spokes are discretised with 10-nodes tetrahedrons with typical dimension of about 8mm. Given the geometry of the wheel, in this case, symmetry cannot be exploited to reduce the dimension of the model. Great care was devoted to the definition of the finite element mesh in order to maximise the stable time increment in the explicit simulation. The smallest stable time increment that has been obtained is of $2.14 \cdot 10^{-8}$ s, the total duration of the simulation step is set long enough to model the total compression and spring-back phase.

3.3.3. $13°$ *lateral impact test*

In this case, the supporting structure is made up by two different parts, namely the steel base and connection rods. The steel base and connection rods are linked by hinges and realise a compliant mechanism connected to the ground by means of four axial springs (Figure 4). The axial springs are characterised by the nonlinear elastic property shown in Figure 12, that approximates the structural response of the rubber bumpers. The curve of Figure 12 was obtained by

Figure 11: Numerical model of the radial impact test with flat striker.

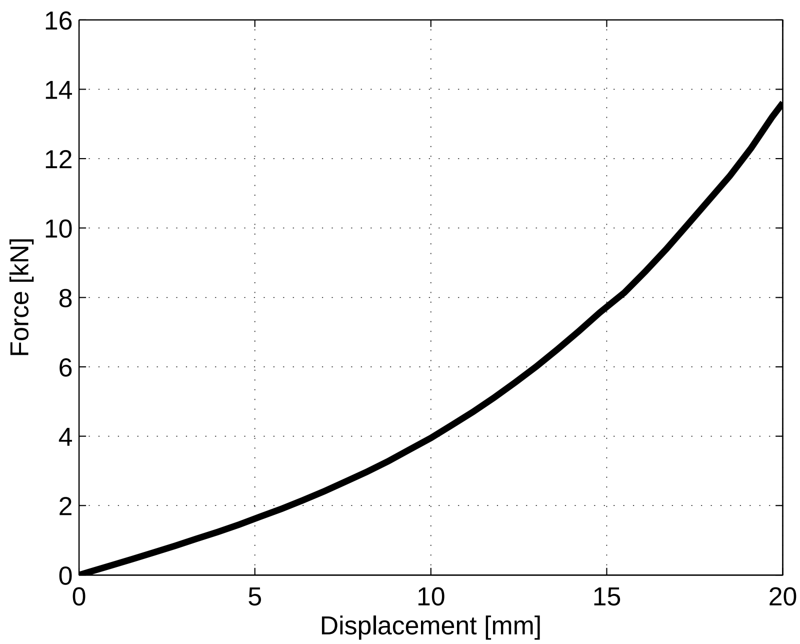

Figure 12: Nonlinear elastic properties of the rubber bumpers of the 13° side impact test.

Figure 13: Numerical model of the 13° side impact test.

adapting data taken from the literature [14]. Additionally, a constant damping factor equal to 1000 Ns/m was assigned to the axial connectors.

The structural compliance of the supporting structure was verified by means of a numerical simulation. By applying a vertical force of 10 kN at the central hub, the resulting deflection computed from the numerical analysis was equal to 7.47 mm, sufficiently close to the 7.5 mm required by the standard [11].

The resulting numerical model of the 13° impact test is shown in Figure 13. Given the geometry of the considered wheel, symmetry is exploited by modelling one half of the structure.

The striker is modelled as a rigid plane with concentrated mass. The tyre structure is discretised with 8-nodes brick elements with typical dimension of about 8 mm, while the wheel rim and spokes are discretised with 10-nodes

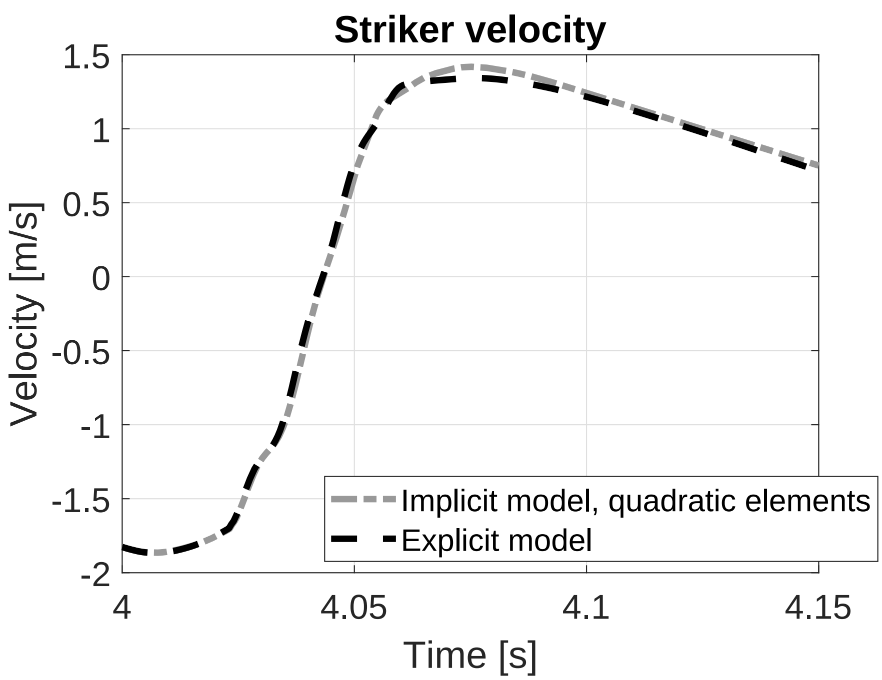

Figure 14: Velocity of the striker calculated with implicit and explicit solver.

tetrahedrons with typical dimension around 8 mm.

As discussed in Sect. 3, this impact can be integrated by a dynamic implicit solver. For the analysis described in this paper, a commercial solver (Abaqus® Standard, release 2019) was used. Figure 14 depicts the velocity time history of the striker calculated both with the implicit and explicit solver. In the comparison, a mesh of linear tetrahedrons has been considered for the explicit model, while, for the implicit one, the same number of elements, but of quadratic order has been analysed. As shown in the picture, the outputs of the models are well aligned.

In Figure 15, a detail of the stress fields at the connection between spoke and wheel rim computed with the two models is depicted. In the picture, the (non-averaged) element Von Mises stress is shown. In the considered area, where a high stress gradient is present, the linear mesh of the explicit model shows a discontinuous field (Figure 15 a), which is not able to represent the stress field in

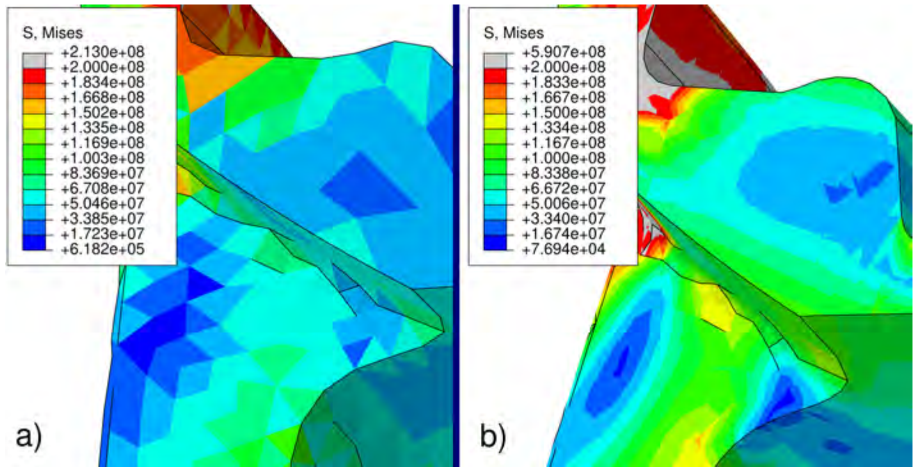

Figure 15: Stress field at the connection between rim and spoke computed with linear mesh and explicit solver (a) and quadratic mesh and implicit solver (b).

a sufficiently accurate way. A better definition is obtained by the quadratic mesh of the implicit model (Figure 15 b). Additionally, the implicit model allows to easily manage local mesh refinements that could be required to further improve the stress definition.

4. Experimental validation

In this section, the models of the three impact tests constructed following the proposed method are experimentally validated. For the validation, experimental tests were conducted on the three impact test benches described in the previous sections. Two different wheel/tyre assemblies were considered for the experimental tests.

For the radial impact with V-shaped striker and the 13° side impact, the 19 inches wheel with ten-spoke style shown in Figure 1 and Figure 4 was employed. The wheel has a five pattern periodicity and is fitted with a 265/50 R19 radial tyre.

For the radial impact test with flat striker, the 20 inches wheel shown in Figure 3 was considered. The wheel is fitted with a 295/30 R20 radial tyre and exhibits a five-spoked structure with bulky spokes.

All the three wheels were instrumented with resistive strain gauges located at the most stressed areas of both the spoke and the rim. The locations of the strain gauges on each wheel depends on the type of impact and will be described in the following sections. To complete the experimental setup, a piezoelectric PCB 353B02 accelerometer was located on the falling mass to measure its vertical acceleration during the impact.

4.1. Radial impact test with V-shaped striker

The present paragraph presents the most significant results obtained from the validation of the radial impact test with V-shaped striker. The reader is addressed to reference [25] for an extended validation and a thorough study of such specific test.

The wheel was instrumented with a set of resistive strain gauges located on the wheel spoke and on the wheel rim, and was placed on the test bench as depicted in Figure 1.

Single axis strain gauges were placed on the front and backside of the wheel spokes as shown in Figure 16. The strain gauges are oriented as the spoke main axis. At the backside of the spoke, near the spoke root, a triaxial strain rosette was employed to analyse the stress state near the fillet.

An additional set of single axis strain gauges was located on the wheel rim as shown in Figure 17. The strain gauges are equally spaced of $9°$ and are positioned as to cover an entire arch of $36°$ on the rim, their measuring axis is kept coincident with the wheel lateral direction.

The tyre inflation pressure was set to 230 kPa. Two different energy levels were tested, namely 700 Joule and 3500 Joule, representing two typical test situations. The energy level is adjusted by changing the mass of the striker and its falling height. The parameters related to the two tests are reported in Table 4. In the 700 Joule test the mass of the striker is 150 kg, falling from a height of 476 mm, while in the 3500 Joule test the mass is 260 kg and the falling height is 1372 mm. The velocity of the striker when impacting the tyre is

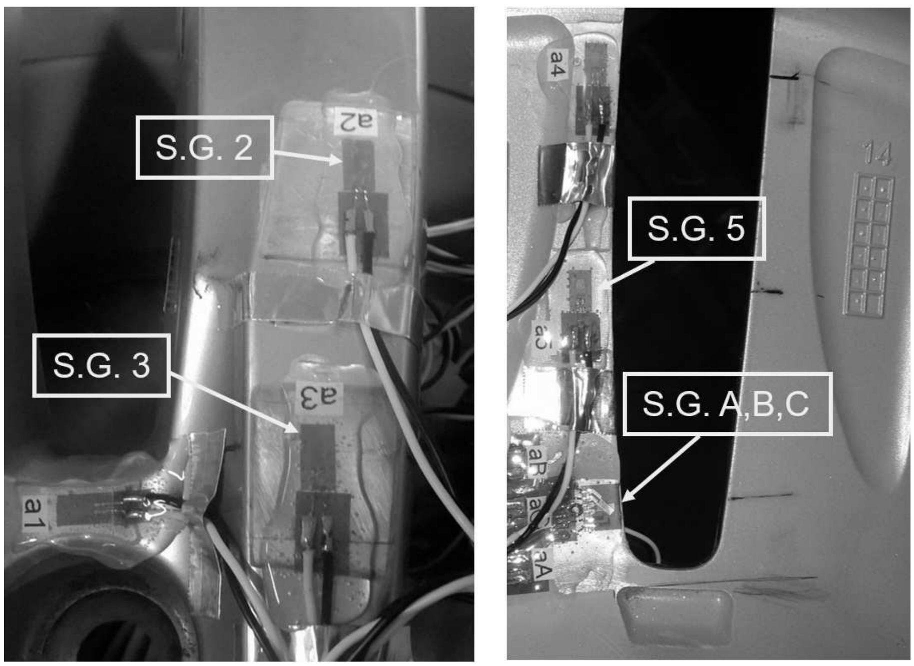

Figure 16: Strain gauges location on front and backside of wheel spoke - radial impact test with V-shaped striker. S.G.2, S.G.3 and S.G.5: single axis strain gauges. S.G.A,B,C: triaxial strain rosette.

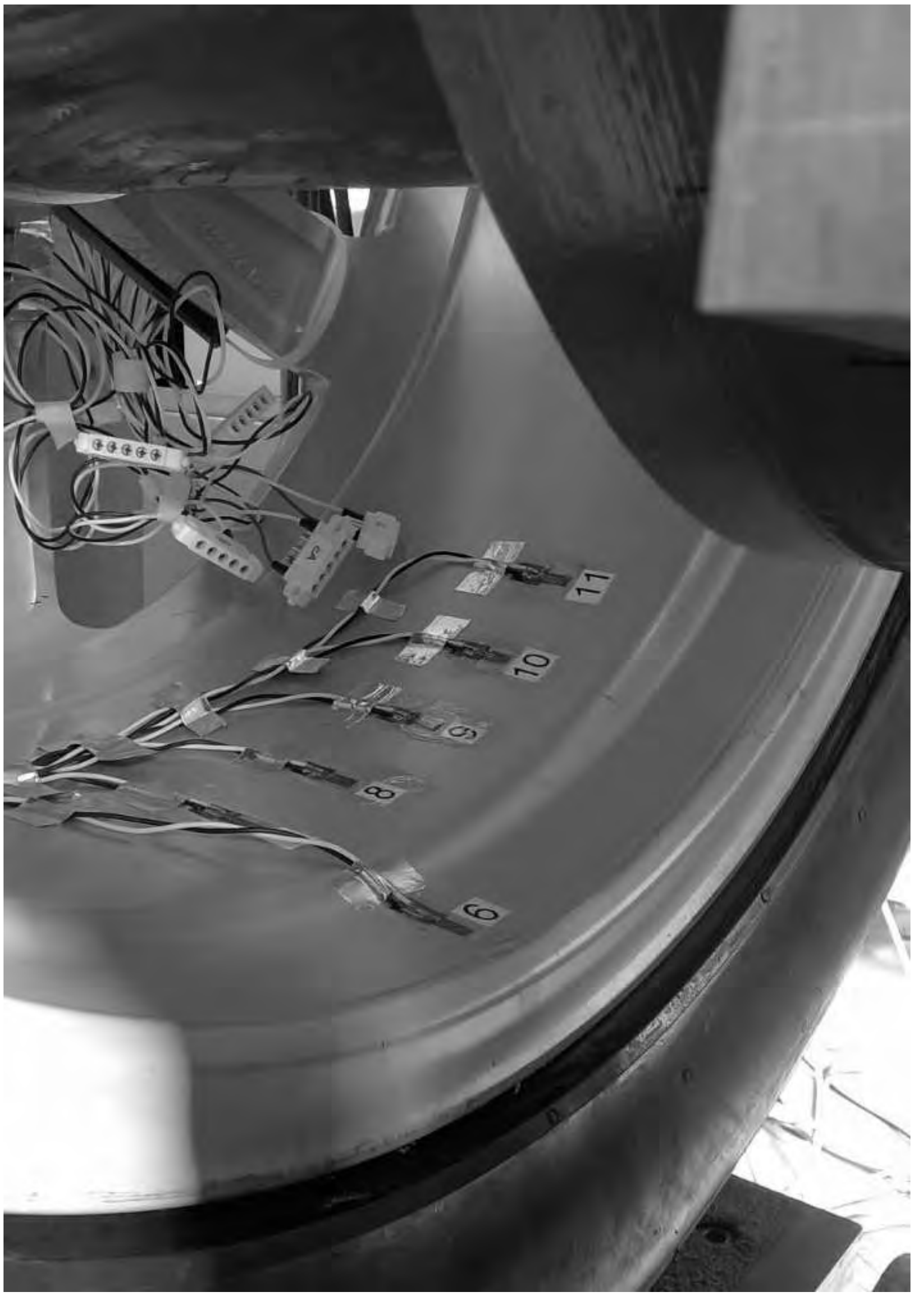

Figure 17: Strain gauges location on the wheel rim - radial impact test with V-shaped striker.

Table 4: Energy levels tested for the radial impact test with V-shaped striker.

Energy (nominal) [J]	Striker mass [kg]	Falling height [m]	Impact velocity (measured) [m/s]	Energy (measured) [J]
700	150	0.476	2.9	631
3500	260	1.372	5.1	3381

recorded by a dedicated sensor integrated in the test bench, so that the actual impact energy of the test can be measured (see Table 4). For the validation of the model, the two impact tests have been simulated by using as input the measured velocities.

Figure 18 depicts the comparison of measured and simulated time histories of the striker acceleration for the 700 Joule and the 3500 Joule test. The acceleration peak is around 15 g for the 700 Joule test and 40 g for the 3500 Joule test. Considering the low energy impact, it is clear from Figure 18 a) that the impact energy is totally absorbed by the tyre deformation, on the other hand, for the high energy test, the tyre sidewalls are completely folded and the striker gets in contact with the rim flanges. This point is highlighted by the slope change in the signals of Figure 18 b) (around 4.02 s). For the low energy test, the numerical model is perfectly matching experimental data, with a difference of less than 1% on the acceleration peak. In the case of the high energy level, the amplitude and shape of the signal is well captured, even if the numerical model tends to overestimate the peak of about 20%.

A good correlation was obtained also for the strain measurements.

On the spoke (Figure 19), the numerical model is able to follow the experimental time histories both for high and low energy levels, with a relative difference of less than 10% on the strain peaks.

On the rim (Figure 20), the trend is confirmed; in this case a slightly larger

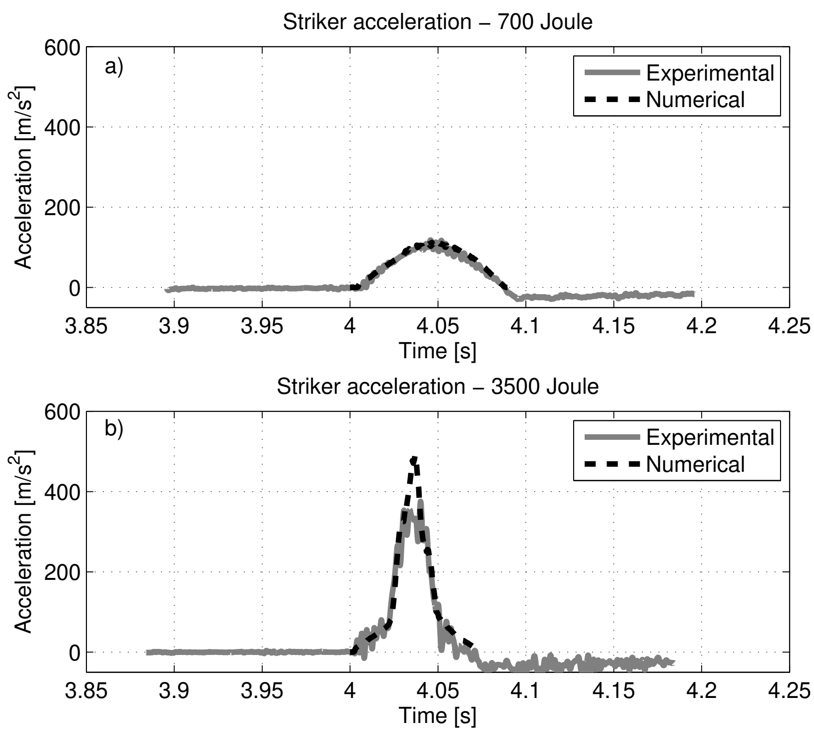

Figure 18: Measured (grey) and simulated (dashed black) time history of the striker acceleration for the two considered energy levels - radial impact test with V-shaped striker.

Table 5: Energy levels tested for the radial impact test with flat striker.

Energy [J]	Striker mass [kg]	Falling height [m]
234	397	0.060
978	997	0.100

difference was obtained for the low energy case, probably due to the small strain values in this condition.

4.2. Radial impact test with flat striker

For this kind of test, the experimental setup is shown in Figure 3. The tyre inflation pressure was set to 250 kPa. Several strain gauges were placed on front and back side of one spoke as reported in Figure 21. The wheel is positioned so as the impact happens exactly in the middle of the window between two consecutive spokes as shown in Figure 3.

Two different energy levels, denoted here as high and low energy levels, were tested; the test parameters are summarised in Table 5.

Figure 22 depicts the comparison between measured and simulated accelerations of the striker. For the low energy test (Figure 22 a)), the impact energy is entirely absorbed by the tyre deformation, while in the high energy case (Figure 22 b)) the striker gets in contact with the rim flanges as highlighted by the slope change around 0.08 s in the graphs of Figure 22 b). In both cases the numerical model turns out to be very accurate in capturing the shapes of the signals and the acceleration peaks. A maximum difference of 15% is found on the acceleration peak for the high energy impact, while for the low energy the difference reduces to 10%.

In Figure 23 the comparison related to the strain signals is reported. All the three strain gauges show a compressive strain state during the impact, the shape of signal time histories is the same of the acceleration ones. The highest strain is measured by S.G. 1, located on the back side of the spoke, closer to the wheel centre (Figure 21 b). The agreement between simulations and measurements is good, the difference on the maximum strain peak is 9% and 11%, respectively for

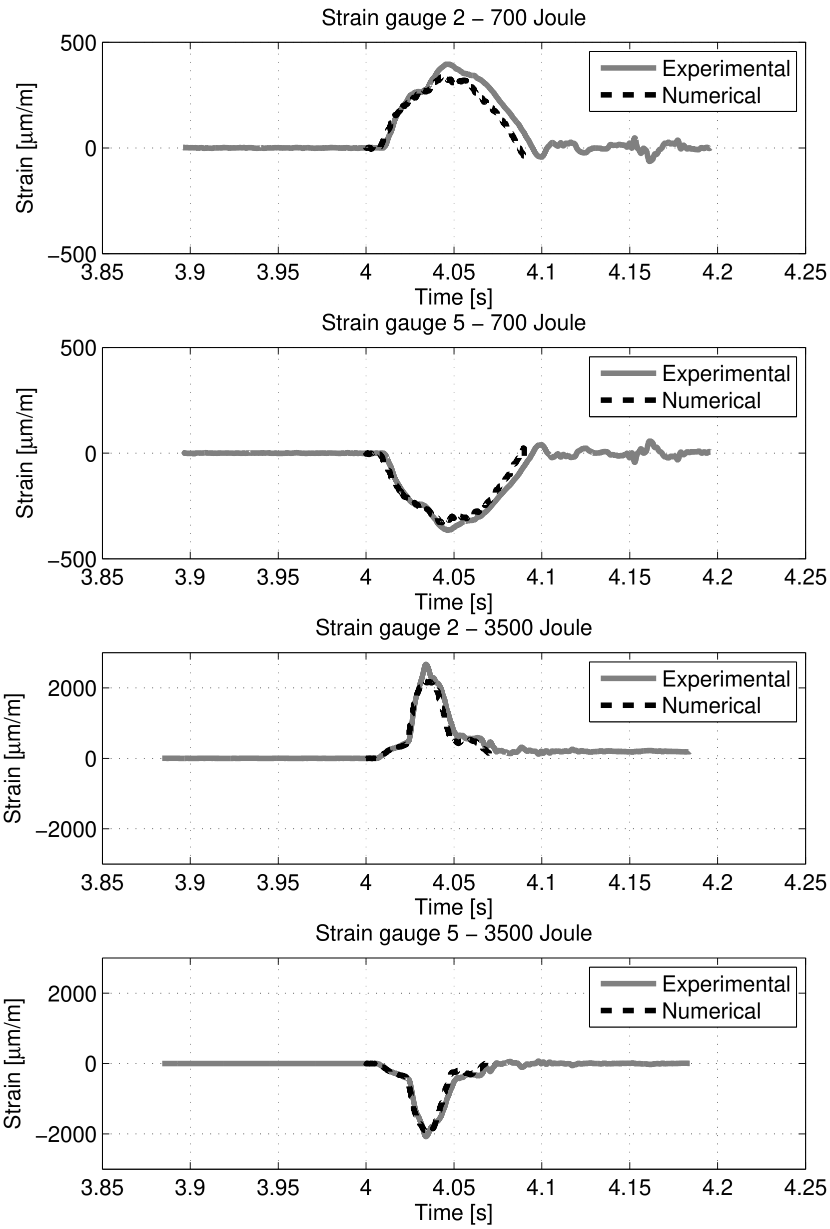

Figure 19: Measured (grey) and simulated (dashed black) time history of the strain at the spoke locations for the two considered energy levels - radial impact test with V-shaped striker.

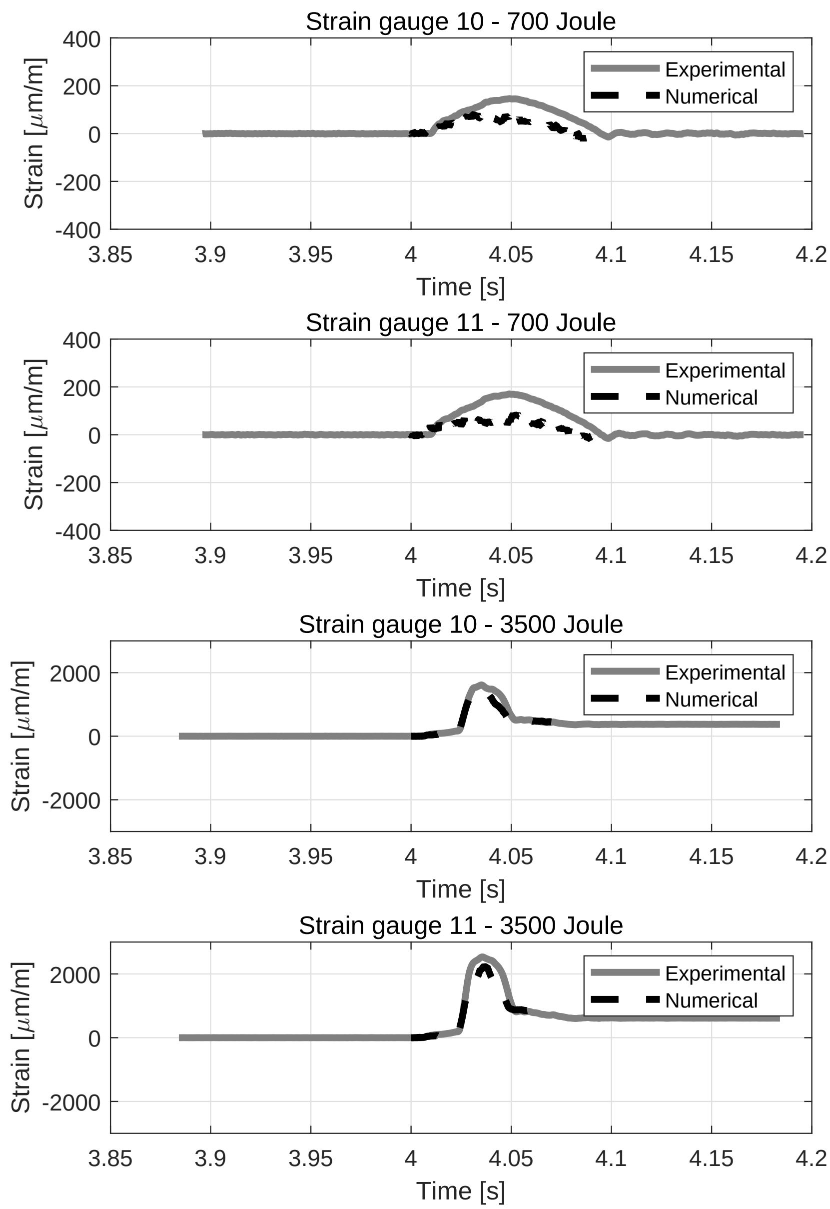

Figure 20: Measured (grey) and simulated (dashed black) time history of the strain at the rim locations for the two considered energy levels - radial impact test with V-shaped striker.

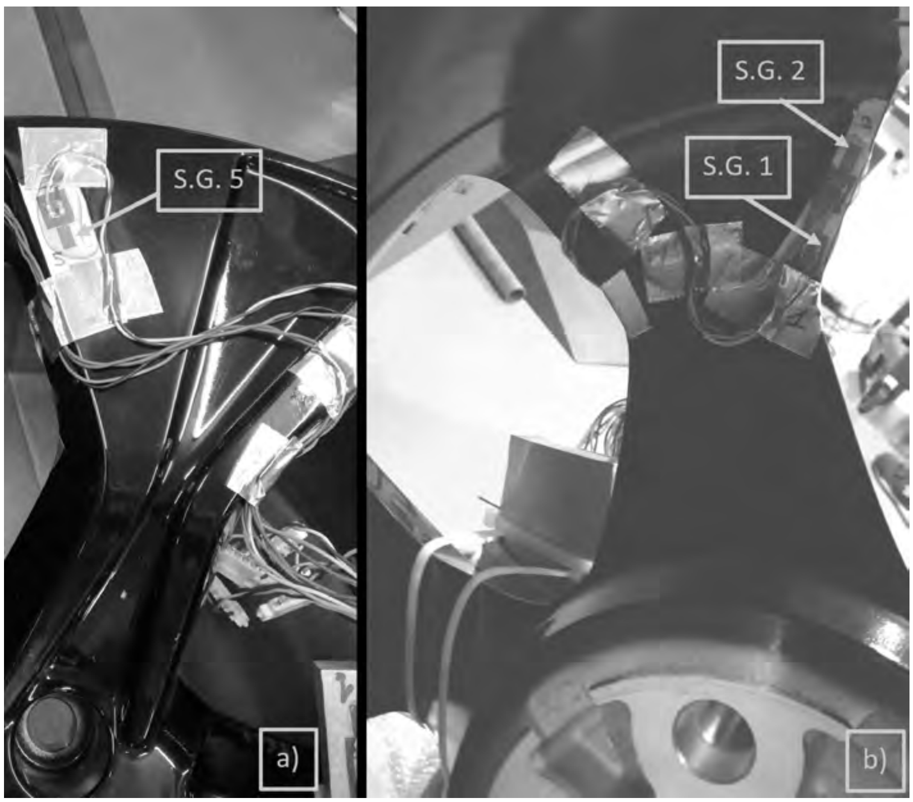

Figure 21: Position of the strain gauges on front (a) and back side (b) of the wheel used in the radial impact test with flat striker.

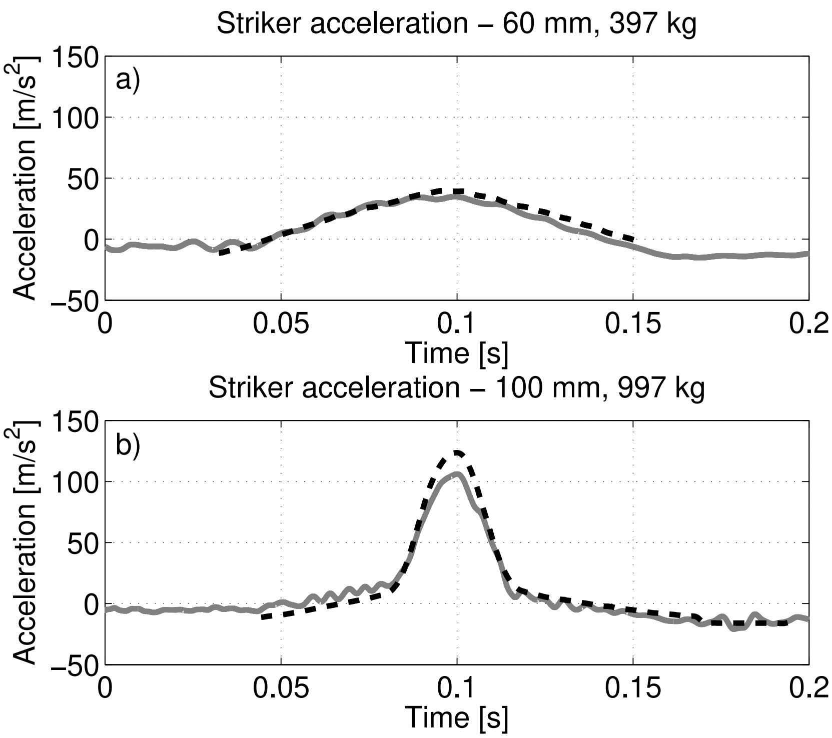

Figure 22: Measured (grey) and simulated (dashed black) time histories of the striker acceleration for the low (a) and high (b) energy level of the radial impact test with flat striker.

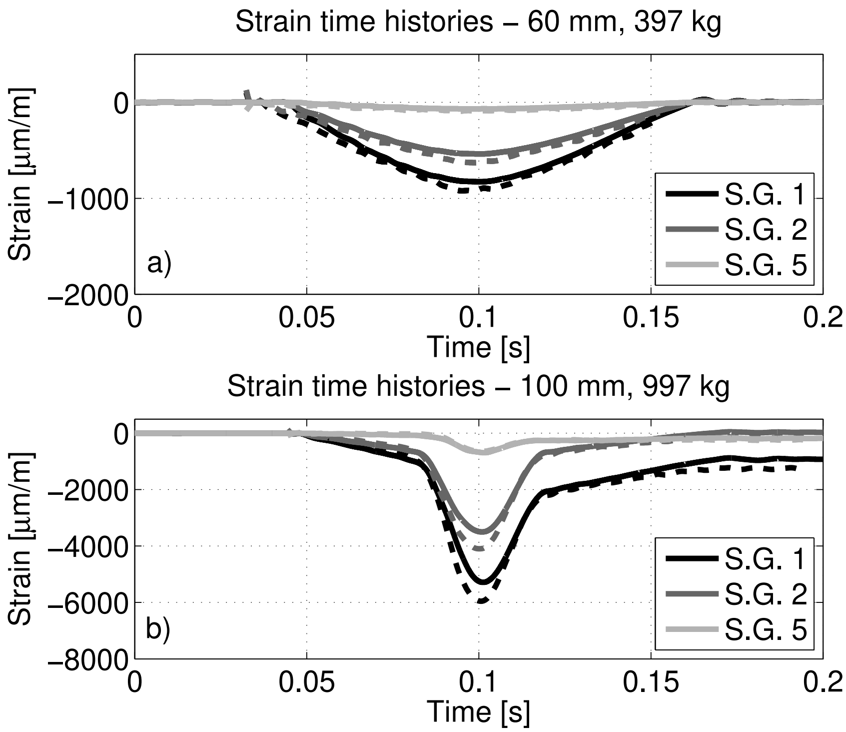

Figure 23: Measured (solid line) and simulated (dashed line) time histories of the strain at the strain gauges locations for the low (a) and high (b) energy level of the radial impact test with flat striker.

the low and high energy impact. The numerical model is slightly overestimating the strain levels.

4.3. 13° *side impact test*

The experimental setup of the 13° side impact test is shown in Figure 4. The same type of wheel used for the radial impact test with V-shaped striker was selected for validation. The wheel was instrumented with resistive strain gauges located on the front and back side of the spokes as depicted in Figure 24.

The wheel is positioned on the test bench so that the impact point is located on two twin spokes as shown in Figure 4.

Figure 24: Position of the strain gauges on front (a) and back side (b) of the wheel used in the 13° side impact test.

Table 6: Energy levels tested for the 13° side impact test.

Energy [J]	Striker mass [kg]	Falling height [m]
830	423	0.200
1500	673	0.230

Two different energy levels, namely high and low energy, were tested; the test parameters are summarised in Table 6.

In Figure 25 a) and b) the time histories of the acceleration of the striker are reported for the low and high energy levels respectively. In the figure, the contact between striker and tyre sidewall starts approximately at 0.05 s; at this instant, the acceleration linearly increases along with the tyre sidewall is progressively deformed. Around 0.07 s the striker gets in contact with the rim flange, at this moment a change in the slope of the acceleration signal is evident. The acceleration peak is similiar for the two energy levels. The numerical model, reported with dashed lines in Figure 25, follows well the experimental data, with a difference of less than 20% on the acceleration peak. A more pronounced obscillation of the numerical acceleration is evident, especially for the low energy impact, probably due to an underestimation of the damping of the rubber bumpers at lower speed.

The accuracy of the numerical model is confirmed also by the comparison on the strain time histories of Figure 26, where the strains measured by strain gauges 3, 4 and 5 are shown and compared with numerical simulations. In the picture, the same trend of the acceleration signal can be highlighted. A tension strain field (positive values) is measured in the front side of the spokes by strain gauge 3, while in the back side of the spoke a compressive strain is measured. For the low energy impact, a maximum strain of 4100 $\mu m/m$ was measured by strain gauge 3. For the high energy test, the maximum strain increases up to 9700 $\mu m/m$ and a significant residual strain remains after this test. From the comparison with the numerical simulations (dashed lines in Figure 26), a good matching can be outlined. The model is able to capture both the shape of the

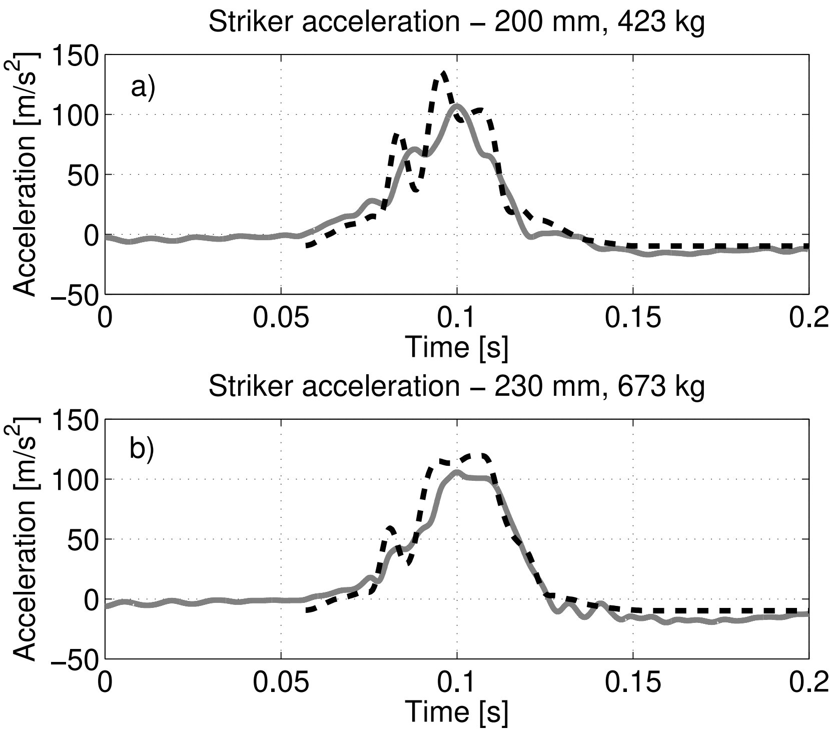

Figure 25: Measured (grey) and simulated (dashed black) time histories of the striker acceleration for the low (a) and high (b) energy level of the 13° side impact test.

strain signals and the peaks. Additionally, for the high energy test (Figure 26 b), the residual strain after the test is correctly replicated by the model.

4.4. Wheel damage

During such kind of impact tests, it is likely that fractures occur at the most critical locations of the wheel. As described in detail by the authors in [25], ductile fracture criteria can be effectively employed to estimate fractures occurence. As supported also by other authors [15], the total plastic work per unit of volume W_p can be used as a damage indicator. This quantity is defined by the integral [15]

$$W_p = \int_0^{\epsilon_f} \sigma_t d\epsilon_p \tag{1}$$

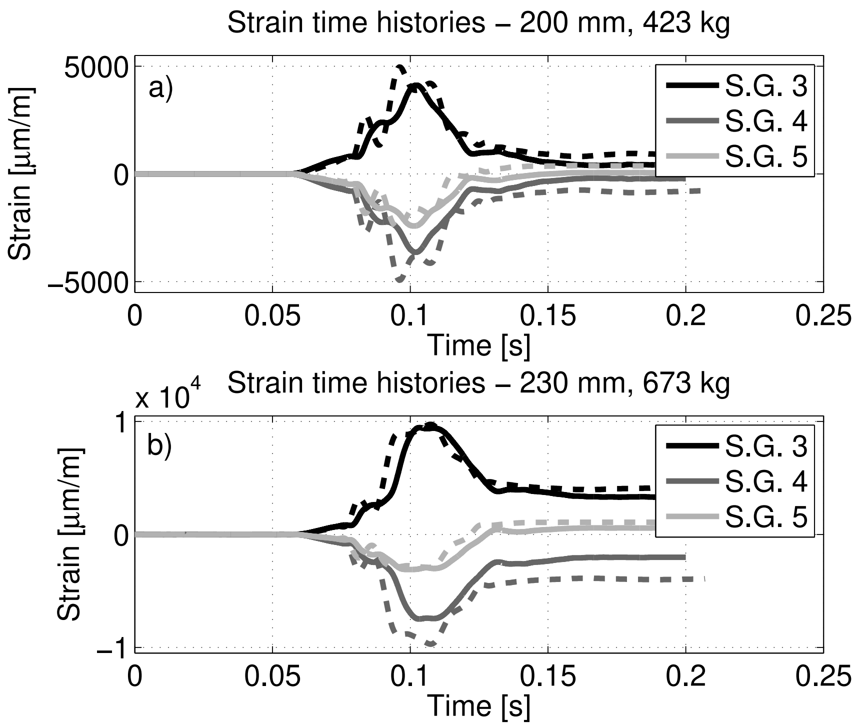

Figure 26: Measured (solid line) and simulated (dashed line) time histories of the strain at the strain gauges locations for the low (a) and high (b) energy level of the 13° side impact test.

Figure 27: Wheel fracture after radial impact test with flat striker. The energy level was 4060 J. Courtesy of "Cromodora Wheels".

where ϵ_f is the true strain at fracture, while σ_t and ϵ_p the true stress and plastic strain respectively. The limit of the quantity in eq. 1 is obtained from the material stress/strain relationship.

Regarding the wheel rims analysed in this paper, the one tested for the radial impact test with flat striker showed the presence of fractures on the wheel rim (Figure 27). In this case, the energy level was equal to 4060 J (striker mass of 1000 kg, falling height 414 mm). As evidenced from Figure 27, the fracture is located on the wheel rim, near the fillet that connects the outer rim flange with the rim structure.

The same condition was simulated with the numerical model described in section 3.3.2. The contour plot of the total plastic work per unit of volume is shown in Figure 28, the values in the scale are nomalised over the material limit, meaning that in the grey areas the limit is exceeded. As evident from the picture, the model foresees a fracture in the correct location; moreover, from the detail of Figure 28 (left) one can see that the extension of the grey

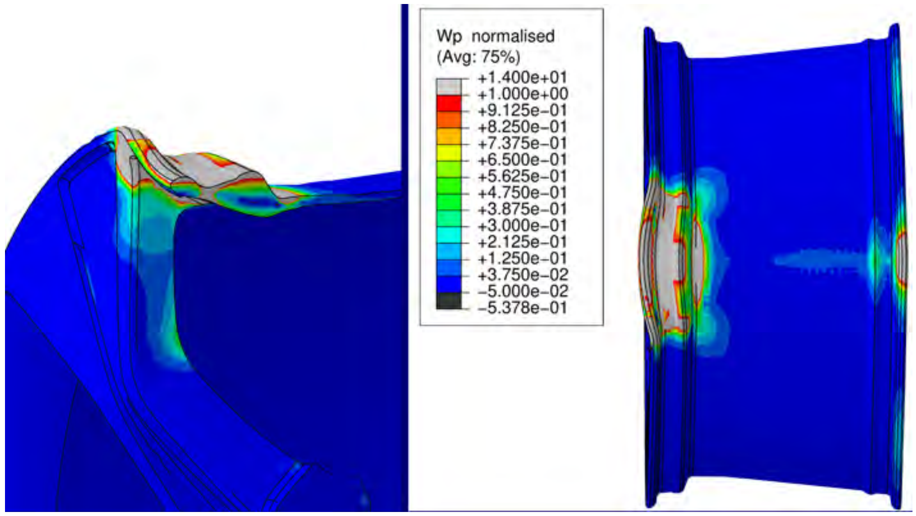

Figure 28: Normalised contour plot of the total plastic work per unit of volume for the radial impact with flat striker and an energy level of 4060 J. In grey areas material limit is exceeded.

area is completely passing through the flange thickness, indicating a plausible separation from the rim structure in this area, exactly as what experienced during the test of Figure 27.

5. Conclusions

In the paper, a comprehensive method for the numerical simulation of indoor impact tests of lightweight aluminium wheels has been presented and discussed. The method provides a well defined procedure for the realization of finite element models able to simulate different impact tests on road vehicle wheels. The models are able to give valuable information to the wheel designer at a reasonable computational time and requiring very few tyre data.

The proposed method has been applied to the analysis of three different types of impact test, namely the radial impact test with V-shaped striker, the radial impact test with flat striker and the 13° side impact test.

For the 13° side impact test, a novel approach in the simulation of the impact has been proposed. In this case, due to the relatively small deformation of the tyre, an implicit solver has been used instead of the explicit solver used in all similar works in the literature. This approach has shown to reduce the computational time of about four times while allowing for a more detailed mesh. This approach has allowed to increase the accuracy of the solution of the stress field in areas of the wheel where a significant stress gradient is present.

A simplified model is proposed for the tyre. The material data required for this simplified model have been taken from the literature; simple deformation and frequency response tests have been presented to tune this data to match the characteristics of the considered tyre. The geometry of the cross section of the tyre has been directly measured. This simplified tyre model is able to capture the main mechanical behaviour of the tyre, without requiring a deep knowledge of the tyre structure and materials, usually not available for the wheel rim designer.

The proposed methodology has been experimentally validated for the three considered impact tests. For the validation, two different kinds of wheels have been considered: a 19 inches with ten spoke style wheel for the radial impact test with V-shaped striker and for the 13° side impact test, and a 20 inches with five spoke style wheel for the radial test with flat striker. The wheels have been instrumented with a set of strain gauges located in the most stressed areas. The acceleration of the striker has been measured by means of a piezoelectric accelerometer. For each test, a low and a high energy impact level has been considered. Results of the validation confirmed the effectiveness of the numerical model in reproducing both the shapes and the maximum values of the acceleration time histories and the strains at the strain gauge locations. Errors always less than 20% have been found in the peak acceleration, while errors of the order of 10% have been found for the deformations. Also, for the high energy impacts, the numerical models correctly compute the residual strain after the impact.

Finally, results show that the plastic strain energy density is a useful indicator to highlight the crack appearance in the wheel rim and spokes.

Acknowledgements

The authors wish to thank ing. Claudio Sorlini from Cromodora Wheels (www.cromodorawheels.it) for the substantial support in the experimental activities.

References

[1] The future of road transport, European Commission, Bruxelles, BEL, european Commission, 2019.

[2] M. GOBBI, G. MASTINU, ANALYTICAL DESCRIPTION AND OPTIMIZATION OF THE DYNAMIC BEHAVIOUR OF PASSIVELY SUSPENDED ROAD VEHICLES, Journal of Sound and Vibration 245 (3) (2001) 457–481, ISSN 0022-460X, doi:\bibinfo{doi}{10.1006/JSVI.2001.3591}, URL `https://www.sciencedirect.com/science/article/pii/S0022460X01935916`.

[3] G. Mastinu, M. Ploechl, Road and Off-Road Vehicle System Dynamics Handbook, CRC Press, Boca Raton., 2014.

[4] L. Guzzella, A. Sciarretta, Vehicle Propulsion Systems, Springer, Berlin, Heidelberg, 2013.

[5] F. Ballo, R. Frizzi, G. Mastinu, D. Mastroberti, G. Previati, C. Sorlini, Lightweight Design and Construction of Aluminum Wheels, in: SAE Technical paper, doi:\bibinfo{doi}{10.4271/2016-01-1575.Copyright}, 2016.

[6] U. Kocabicak, M. Firat, Numerical analysis of wheel cornering fatigue tests, Engineering Failure Analysis 8 (4) (2001) 339–354, ISSN 13506307, doi:\bibinfo{doi}{10.1016/S1350-6307(00)00031-5}.

[7] M. Firat, R. Kozan, M. Ozsoy, O. H. Mete, Numerical modeling and simulation of wheel radial fatigue tests, Engineering Failure Analysis 16 (5) (2009) 1533–1541, ISSN 13506307, doi:\bibinfo{doi}{10.1016/j.engfailanal.2008.10.005}.

[8] X. Wan, Y. Shan, X. Liu, H. Wang, J. Wang, Simulation of biaxial wheel test and fatigue life estimation considering the influence of tire and wheel camber, Advances in Engineering Software 92 (2016) 57–64, ISSN 09659978, doi:\bibinfo{doi}{10.1016/j.advengsoft.2015.11.005}, URL `http://linkinghub.elsevier.com/retrieve/pii/S0965997815001714`.

[9] F. M. Santiciolli, R. Möller, I. Krause, F. G. Dedini, Simulation of the scenario of the biaxial wheel fatigue test, Advances in Engineering Software 114 (2017) 337–347, ISSN 0965-9978, doi:\bibinfo{doi}{10.1016/J.ADVENGSOFT.2017.08.006}, URL `https://www.sciencedirect.com/science/article/pii/S0965997817304350`.

[10] L. D. Nurkala, R. S. Wallace, Development of the SAE Biaxial Wheel Test Load File, in: SAE 2004 World Congress & Exhibition, SAE International, ISBN 0768013194, doi:\bibinfo{doi}{10.4271/2004-01-1578}, 2004.

[11] SAE J175, Wheels - Lateral Impact Test Procedure, Tech. Rep., SAE Standards, 2018.

[12] ISO 7141, Road Vehicles - Light Alloy wheels - Impact test, ISO, International Standard Organization, 2005.

[13] Räder – Anforderungen und Prüfungen, Arbeitskreis Lastenheft, Arbeitskreis-Lastenheft AK-LH 08, arbeitskreis der Firmen: Audi AG, Bayerische Motorenwerke AG, DaimlerChrysler AG, Porsche AG, Volkswagen AG, 2006.

[14] X. Wan, X. Liu, Y. Shan, E. Jiang, H. Yuan, Numerical and experimental investigation on the effect of tire on the 13ô impact test of automotive wheel, Advances in Engineering Software 133 (2019) 20–27, ISSN 0965-9978, doi:\bibinfo{doi}{10.1016/J.ADVENGSOFT.2019.04.005}, URL `https://www.sciencedirect.com/science/article/pii/S0965997818308305`.

[15] C.-L. Chang, S.-H. Yang, Simulation of wheel impact test using finite element method, Engineering Failure Analysis 16 (5) (2009) 1711–1719, ISSN 1350-6307, doi:\bibinfo{doi}{https://doi.org/10.1016/j.engfailanal.2008.12.010}, URL `http://www.sciencedirect.com/science/article/pii/S1350630709000028`.

[16] M. Cerit, Numerical Simulation of Dynamic Side Impact Test for an Aluminium Alloy Wheel, Scientific Research and Essays 5 (18) (2010) 2694–2701, ISSN 19922248.

[17] R. Shang, W. Altenhof, N. Li, H. Hu, Wheel impact performance with consideration of material inhomogeneity and a simplified approach for modeling, International Journal of Crashworthiness 10 (2) (2005) 137–150, ISSN 13588265, doi:\bibinfo{doi}{10.1533/ijcr.2005.0333}, URL `https://www.tandfonline.com/doi/pdf/10.1533/ijcr.2005.0333?needAccess=true`.

[18] M. B. K, S. Vinothkumar, S. Sabarinathan, N. AnilKumar, Simulation and test correlation of wheel radial fatigue test, in: SAE Technical Papers, ISSN 2688-3627, doi:\bibinfo{doi}{10.4271/2013-01-1198}, 2011.

[19] M. Zhu, B. Han, Analysis of impact test of aluminum disc wheels based on FEM, in: SAE Technical Papers, ISSN 26883627, doi:\bibinfo{doi}{10.4271/2007-01-3648}, 2007.

[20] M. R. Chauhan, G. Kotwal, A. Majge, Numerical Simulation of Tire and Wheel Assembly Impact Test Using Finite Element Method, in: SAE Technical Paper 2015-26-0186, SAE International, ISSN 0148-7191, doi:\bibinfo{doi}{https://doi.org/10.4271/2015-26-0186}, URL `https://doi.org/10.4271/2015-26-0186`, 2015.

[21] Q. Gao, Y. Shan, X. Wan, Q. Feng, X. Liu, 90-degree impact bench test and simulation analysis of automotive steel wheel, Engineering Failure Analysis 105 (2019) 143–155, ISSN 1350-6307, doi:\bibinfo{doi}{10.1016/J.

ENGFAILANAL.2019.06.097}, URL https://www.sciencedirect.com/science/article/pii/S1350630718315735.

[22] S. Bandral, S. Singh, Impact Analysis of Car Alloy Wheel Rim using Finite Element Analysis, International Journal of Engineering Research & Technology (IJERT) 6 (16) (2018) 1–4.

[23] S. Ishikawa, Y. Sakai, N. Nosaka, Application of Impact Analysis for Aluminum Wheel with Inflated Tire, in: Proceedings of 2014 SIMULIA Community Conference, 2014.

[24] R. R. V. Neves, G. B. Micheli, M. Alves, An experimental and numerical investigation on tyre impact, International Journal of Impact Engineering 37 (6) (2010) 685–693, ISSN 0734-743X, doi:\bibinfo{doi}{https://doi.org/10.1016/j.ijimpeng.2009.10.001}, URL http://www.sciencedirect.com/science/article/pii/S0734743X09001821.

[25] G. Previati, F. Ballo, M. Gobbi, G. Mastinu, Radial impact test of aluminium wheels—Numerical simulation and experimental validation, International Journal of Impact Engineering 126 (January) (2019) 117–134, ISSN 0734743X, doi:\bibinfo{doi}{10.1016/j.ijimpeng.2018.12.002}, URL https://doi.org/10.1016/j.ijimpeng.2018.12.002.

[26] F. Ballo, R. Frizzi, M. Gobbi, G. Mastinu, G. Previati, C. Sorlini, Numerical and Experimental Study of Radial Impact Test of an Aluminum wheel - towards industry 4.0 virtual process assessment, in: Proceedings of the ASME 2017 International Design Engineering Technical Conferences and Computers and Information in Engineering Conference, Cleveland, Ohio, USA, 1–10, doi:\bibinfo{doi}{10.1115/DETC2017-67703}, 2017.

[27] A. L. Costa, F. A. Cardoso, Finite elements simulation of impact in a passenger car tyre, in: SAE Technical Papers, ISSN 26883627, 1–7, doi:\bibinfo{doi}{10.4271/2007-01-2878}, 2007.

[28] S. Taheri, C. Sandu, S. Taheri, Finite Element Modeling of Tire Transient Characteristics in Dynamic Maneuvers, SAE International Journal of Passenger Cars - Mechanical Systems 7 (1) (2014) 221–230, ISSN 19464002, doi:\bibinfo{doi}{10.4271/2014-01-0858}.

[29] H. Zhou, G. Wang, Y. Wang, Wide-base tire-building process and design optimization using finite element analysis, Tire Science and Technology 46 (4) (2018) 242–258, ISSN 00908657, doi:\bibinfo{doi}{10.2346/tire.18.460405}.

[30] O. C. Zienkiewicz, R. L. Taylor, The Finite Element Method, vol. 3: Fluid Dynamics, Butterworth Heinemann, fifth edn., 2000.

[31] K. Balakrishnan, A. Sharma, R. Ali, Comparison of Explicit and Implicit Finite Element Methods and its Effectiveness for Drop Test of Electronic Control Unit, Procedia Engineering 173 (2017) 424–431, ISSN 18777058, doi:\bibinfo{doi}{10.1016/j.proeng.2016.12.042}.

[32] E. Tönük, Y. Ünlüsoy, Prediction of automobile tire cornering force characteristics by finite element modeling and analysis, Computers & Structures 79 (13) (2001) 1219–1232, ISSN 0045-7949, doi:\bibinfo{doi}{10.1016/S0045-7949(01)00022-0}, URL https://www.sciencedirect.com/science/article/pii/S0045794901000220.

[33] F. Ballo, G. Previati, M. Gobbi, G. Mastinu, Tire-rim interaction, a semi-analytical tire model, Journal of Mechanical Design 00000 (2018) 1–12, ISSN 1050-0472, doi:\bibinfo{doi}{10.1115/1.4038927}, URL http://mechanicaldesign.asmedigitalcollection.asme.org/article.aspx?doi=10.1115/1.4038927.

[34] F. Ballo, G. Previati, M. Gobbi, G. Mastinu, A SEMI-ANALYTICAL TYRE MODEL FOR THE STUDY OF TYRE/RIM INTERACTION ON A ROAD VEHICLE, in: Proceedings of the ASME 2017 International Design Engineering Technical Conferences & Computers and Information in

Engineering Conference IDETC/CIE 2017, Cleveland, Ohio, USA, 1–12, 2017.

[35] S. Rao, Mechanical Vibrations, Prentice Hall, 2011.

[36] R. Shang, W. Altenhof, H. Hu, N. Li, Kinetic energy compensation of tire absence in numerical modeling of wheel impact testing, in: SAE Technical Papers, 724, ISSN 2688-3627, doi:\bibinfo{doi}{10.4271/2005-01-1825}, 2005.

[37] R. G. Pelle, FEM Simulation of the Tire/Rim Seating Process, Tire Science and Technology 22 (2) (1994) 76–98, ISSN 0090-8657, doi:\bibinfo{doi}{10. 2346/1.2139537}.